



Autonomous transfer robot system for commercial vehicles at Ro-Ro terminals

Lin Zhang^{a,b}, Yongkang Xu^{a,b}, Jinge Si^{a,b}, Runjiao Bao^{a,b}, Yichen An^{a,b}, Shoukun Wang^{ID a,b,*}, Junzheng Wang^{a,b}

^a School of Automation, Beijing Institute of Technology, 100081, Beijing, China

^b Key Laboratory of Intelligent Control and Decision of Complex Systems, Beijing Institute of Technology, 100081, Beijing, China

ARTICLE INFO

Keywords:

Autonomous transfer of commercial vehicles
Straddle-structured robots
Robot system
Scheduling planning
Autonomous docking

ABSTRACT

With the rapid development of smart port infrastructure, ports such as Rotterdam and Ningbo have made significant progress in automating container handling. However, traditional manual transfer methods at roll-on/roll-off (Ro-Ro) terminals can no longer meet the growing demands for low-cost, high-efficiency, and standardized operations, driven by increased port throughput, labor shortages, and operational complexity. This study introduces a novel autonomous robot transfer system comprising commercial vehicle transfer robots, a cloud scheduling system, and robotic operation systems. An electric transfer robot with independent four-wheel drive and steering was developed for heavy-duty commercial vehicle transfers, featuring a modular software architecture with cloud-based scheduling and planning, and robot perception and control modules. To support multi-robot cooperative transfer in open yard environments, we propose a task allocation algorithm based on an adaptive particle swarm genetic algorithm and an enhanced conflict-aware path planning method under kinematic constraints. For precise and safe vehicle pick-up and drop-off under complex conditions, a multi-stage fusion algorithm is introduced for vehicle body localization, orientation estimation, and wheel alignment, together with a predictive docking control algorithm using virtual transfer vehicle tracking. The system was deployed at the Ro-Ro terminal of Yantai Port, Shandong Province, China, where targeted experiments were conducted. Results demonstrate centimeter-level accuracy in vehicle handling, a transfer efficiency of 91% compared to manual operations, and the operating time reaches 2–3 times. These findings validate the effectiveness and practical value of the proposed robot system and its key technologies.

1. Introduction

Recent advances in AI and digital technologies have driven the development of autonomous and intelligent port logistics (Bonab, Ghoushchi, Deveci, & Haseli, 2023; Li et al., 2023; Zhang, Chen, & Guo, 2023b). Most existing systems focus on container terminals, such as those in Rotterdam, Hamburg, and Ningbo Zhoushan, where AGVs and gantry cranes enable automated horizontal transport (Jiao, Huang, Song, Li, & Wang, 2024; Naeem, Gheith, & Eltawil, 2023; Tsolakis, Zisis, Paefthimiou, & Korfatis, 2022). In contrast, commercial vehicle logistics at roll-on/roll-off (Ro-Ro) terminals face unique challenges, including high vehicle value, dense and irregular parking layouts, and dynamically changing yard and roadway conditions. As a result, current operations still rely heavily on manual labor, leading to high costs, inefficiencies, and a lack of standardization (Chen et al., 2021; Zhang, Chen, & Mei,

2023a; Zhang, Ming, & Chen, 2018). To address these issues, there is a pressing need to develop an intelligent, safe, efficient, low-carbon, and standardized robotic system for fully autonomous commercial vehicle transfer in port environments.

Several autonomous transport solutions for commercial vehicles have been explored. FAW Logistics uses intelligent vehicles on dedicated lanes with vehicle-road coordination, but the system is limited by fixed routes and low flexibility (Lina, Zhihao, Ying, Yue-feng, & Wancong, 2020). COSCO Shipping and Taicang Port developed a foldable frame system for stacked vehicle transport (Weifeng, Qicheng, & Yanjie, 2023), though it remains labor-intensive and inefficient. Stanley Robotics introduced the “Stanley” parking robot (Carlos, Williams, & Pelourdeau, 2023; Polack, Dallen, & Cord, 2020), yet its compact size limits its use in dense terminal environments. In contrast, container terminals achieve high efficiency through coordinated AGVs and cranes on fixed routes

* Corresponding author.

E-mail addresses: bit.zhanglin@bit.edu.cn (L. Zhang), yongkang.xu@bit.edu.cn (Y. Xu), bit_si_jin_ge@bit.edu.cn (J. Si), 3120230765@bit.edu.cn (R. Bao), bit_anyichen@bit.edu.cn (Y. An), bitwsk@bit.edu.cn (S. Wang), wangjz@bit.edu.cn (J. Wang).

(Chen et al., 2020; Li, Cai, He, & Guo, 2024). However, autonomous transfer of commercial vehicles presents unique challenges: it demands mobile equipment capable of navigating confined spaces, accurately positioning and docking with target vehicles, and supporting multi-robot cooperative scheduling in open, unstructured yards.

Current commercial vehicle transfer equipment primarily relies on carrier plate lifting mechanisms or multi-wheel independent “gripping” wheels. For instance, Endo et al. (2008), Kashiwazaki et al. (2011) proposed the iCART and iCART II systems, which utilize four independent robots to grasp car tires for vehicle transfer. Slanina, Pergl, and Kedron (2022) proposed a pallet transport system capable of omnidirectional movement and in-place rotation, while Pan, Yan, Zhou, Cai, and Lu (2020) designed a bidirectional autonomous guided vehicle for indoor parking lots. However, these systems are predominantly designed for indoor environments and are unsuitable for outdoor storage yards at ports. They are unable to accommodate the demands of high-speed transfers in compact parking spaces or on uneven terrain.

In multi-robot task scheduling and planning, the process is typically divided into task assignment and path planning (Wang, Wang, & Han, 2024; Wang et al., 2025). For task assignment, existing solutions often formulate as a multi-constrained optimization problem, solving it through advanced intelligent optimization algorithms such as particle swarm optimization (Ran, Liu, Zhang, & Cheng, 2025; Wu, Wang, & Chen, 2024), genetic algorithms (Liu et al., 2025), and ant metaheuristic methods (Zhao, Song, Jiang, Wang, & Dong, 2024). For path planning, search-based (Kottinger, Almagor, & Lahijanian, 2022; Wen, Liu, & Li, 2022) and optimization algorithms (Yang, Ge, Zheng, & Zeng, 2025; Zang et al., 2023, 2024) are commonly employed. For example, Li et al. (2021) proposed a novel rolling horizon collision resolution framework to generate high-quality solutions for complex, crowded warehouses. In the context of AGVs scheduling and bidirectional conflict-free path planning at port container terminals, Cao, Yang, Liu, Zeng, and Chen (2023) introduced a double-layer mixed-integer programming model and achieved conflict-free AGVs scheduling for large-scale container transport using a two-layer differential evolution algorithm for dynamic routing. However, the traditional logistics AGVs system is relatively simple, with fixed driving and parking operation areas. In contrast, at Ro-Ro docks, the layout of the yard and roads is dynamic and flexible. Thus, the planning process must account not only for the kinematic model, shape, and size of the transfer robot but also for dynamic scheduling based on the changing parking positions of commercial vehicles in the yard.

The positioning and docking of commercial vehicles can typically be divided into two stages: target detection and positioning, and docking tracking control. For target detection and positioning, approaches are generally categorized into traditional methods (Xu, Wang, Wang, Lin, & Liang, 2023; Xu, Chen, Deng, Wang, & Wang, 2024) and deep learning-based methods (Chen & Li, 2022; Zhou et al., 2025). For instance, Ding, Ming, and Wang (2023) proposed a hull-based vehicle pose estimation algorithm alongside an attitude estimation criterion that minimizes occlusion areas. Jin et al. (2023) introduced a vehicle detection algorithm that combines clustering results with deep learning to reliably detect vehicle targets. In docking tracking control, research is mainly focused on two strategies: real-time target attitude detection and correction using sensing systems, and global path planning based on initial position detection (Liu et al., 2022; Wang, Shan, Yue, & Wang, 2020). For example, Gong et al. (2022) developed a real-time layered planner, consisting of path and trajectory planning stages, that enables automatic docking control of wireless charging stations using fast nonlinear model predictive control. Cai, Zhang, Yang, Wang, and Shi (2023) designed trajectory planning technology for the automatic docking of unmanned ships using UWB positioning. However, in port yard loading and unloading scenarios, the parking distances between commercial vehicles are small and fixed, requiring strict accuracy in loading and unloading operations. Additionally, traffic constraints in narrow spaces and challenging, variable weather conditions must be considered.



Fig. 1. Autonomous transfer solutions for commercial vehicles: (a) Straddle structure transfer robot; (b) The robot travels through the narrow yard; (c) Robot rainy day pick-up operation; (d) Multi-robot transfer operation.

To address these limitations, as shown in Fig. 1, this paper presents a robotic system for autonomous operation in Ro-Ro terminals. While previous studies have explored fixed-lane navigation (Lina et al., 2020), foldable-frame handling (Weifeng et al., 2023), and automated parking systems (Polack et al., 2020), these approaches are constrained by infrastructure rigidity, labor intensity, or scalability issues, and do not achieve full autonomy in vehicle pick-up, transfer, and drop-off within unstructured terminal environments. To the best of our knowledge, this is the first comprehensive realization of autonomous commercial vehicle transfer under real-world Ro-Ro terminal conditions. The main contributions are as follows:

- (1) We propose an autonomous robot system for transferring commercial vehicles, comprising commercial vehicle transfer robots, the cloud scheduling system, and the robotic operation system. This system is successfully deployed at the Ro-Ro terminal of Yantai Port in Shandong Province, China, where its effectiveness and practicality are validated.
- (2) A commercial vehicle electric autonomous transfer device has been designed with a “straddle-type” structure, integrating a composite clamping mechanism and an independent four-wheel drive and steering system. It can realize multi-modal high-speed driving, such as self-rotation and lateral movement in complex terrain, while passing through a narrow space and clamping different types of commercial vehicles.
- (3) We develop a task allocation algorithm based on an adaptive particle swarm genetic algorithm, alongside an enhanced conflict search path planning algorithm under kinematic constraints, which facilitates conflict-free cooperative transfer of multiple vehicles in a dynamic yard environment.
- (4) We propose a multi-stage fusion algorithm for vehicle body positioning, orientation, and wheel alignment, as well as a predictive control algorithm for robot docking based on virtual transfer vehicle tracking, achieving precise docking and safe pick-up and drop-off vehicles in compact yards.

The rest of this article is organized as follows. Section 2 outlines the robot system for the autonomous transfer of commercial vehicles. Our cloud scheduling planning algorithm and robotic pick-and-place operation algorithm are described in Sections 3 and 4, respectively. Section 5 is the deployment and Experiment in the actual environment, and Sections 6 and 7 are the discussion and conclusion.



Fig. 2. The layout of the Ro-Ro terminal and the current status of commodity transshipment operations.

2. Overview of robot system for autonomous transfer of commercial vehicles

2.1. Transport operation scenario analysis

As shown in Fig. 2, Ro-Ro terminals are typically divided into specialized zones such as loading/unloading areas, yards, stereo garage, and distribution ports. Loading/unloading areas accommodate recently imported and soon-to-be-exported commercial vehicles, while yards and multi-story garages store imported vehicles awaiting departure and those destined for export. Distribution ports facilitate the transfer of commercial vehicles between the terminal and external roll-on vehicles. Currently, commercial vehicle transfer involves manual operations, requiring the involvement of multiple roles like tally clerks, transfer drivers, traffic controllers, transport vehicle drivers, and inspectors. This process is plagued by high costs, lengthy procedures, and environmental pollution, necessitating urgent intelligent transformation. There are several challenges to achieving fully autonomous commercial vehicle transport:

- Autonomous transfer equipment must have the ability to move with heavy loads, high speeds, and flexibility in dense and complex storage yards, and be able to transfer commercial vehicles of different models.
- Dynamic and efficient scheduling systems are needed to dynamically and efficiently schedule the transfer equipment according to the parking position of the commodity vehicles in the yard and roads with free and flexible layout.
- The transfer equipment needs to accurately and safely pick up and place commodity vehicles in a small space in the harsh and changeable port environment.

Moreover, emphasizing safety, environmental adaptability, and compact, modular hardware and software design is crucial due to the high value and demanding operational conditions of commercial vehicles.

2.2. System overview

To enable autonomous transfer of commercial vehicles at Ro-Ro terminals, a robotic system is proposed, as shown in Fig. 3. The system in-

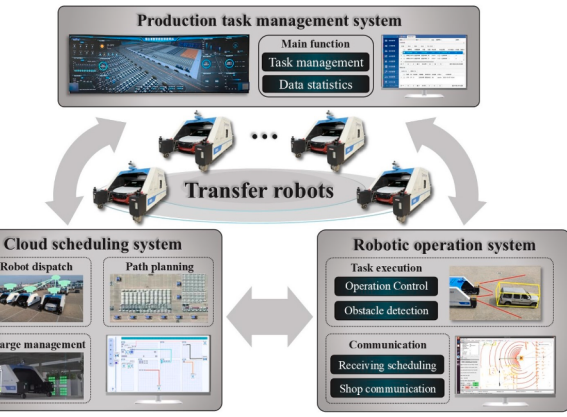


Fig. 3. Overall architecture of robot system for autonomous transport of commercial vehicles.

tegrates with the port's existing task management framework and comprises commercial vehicle transfer robots, a cloud scheduling system, and robot operation units. The task management and cloud scheduling systems are hosted on remote servers, while the operation units are embedded in each robot. The port's task management system organizes internal logistics and generates commercial vehicle transfer plans. The cloud scheduling system then assigns tasks and optimizes path planning for multiple robots, communicating instructions to the robotic units. Using these global path directions, the robots employ perception, localization, control, and drive modules to autonomously execute pick-up and drop-off tasks. Each robot reports task completion in real-time, updating the vehicle's current location.

2.3. Robot hardware composition

To enable flexible maneuvering and placement of commercial vehicles in densely packed storage yards, a heavy-duty electric robot with a "straddle-type" double-body structure is designed, as illustrated in Fig. 4 and detailed in Table 1. The robot is constructed from Q355B low-alloy, high-strength structural steel and features independent four-wheel drive and steering systems. Each wheel is equipped with a dedicated drive motor and steering motor, allowing for multimodal mobility, including in-place rotation, lateral movement, and Ackermann steering, through individual control of the four pairs of motors. Additionally, a modular, integrated, and adaptive clamping assembly mechanism is developed, which automatically adjusts its position based on the wheelbase of the commercial vehicle. This design accommodates the clamping and transfer of commercial vehicles with varying wheelbase sizes.

Building on the aforementioned mechanical mechanism, the transfer robot for autonomous commercial vehicle transport also includes a perception and positioning unit, a robot-side control unit, and a drive execution unit. The perception and positioning unit consists of a top-mounted multi-line LiDAR, surrounding multi-line LiDARs, internal single-line LiDARs, network cameras, a posture sensor, and a global satellite navigation system (GNSS). The top-mounted LiDAR, posture sensor and GNSS enable multi-sensor fusion for self-positioning within the yard, while the surrounding LiDARs provide omnidirectional obstacle detection and vehicle localization. The internal single-line LiDARs are specifically used to position the wheels of the commercial vehicle during the pick-up phase. At the core of the robot control unit is an x86 CPU-based main controller. It gathers and processes information from the cloud and the perception and positioning unit then relays this data to the underlying controller. The controller converts the information into actionable control signals for the drive execution unit, facilitating system-level decision-making and control. The drive execution unit consists of servo drivers, drive motors, steering motors, wheelbase adjustment motors, vertical lifting motors, and clamping motors. The

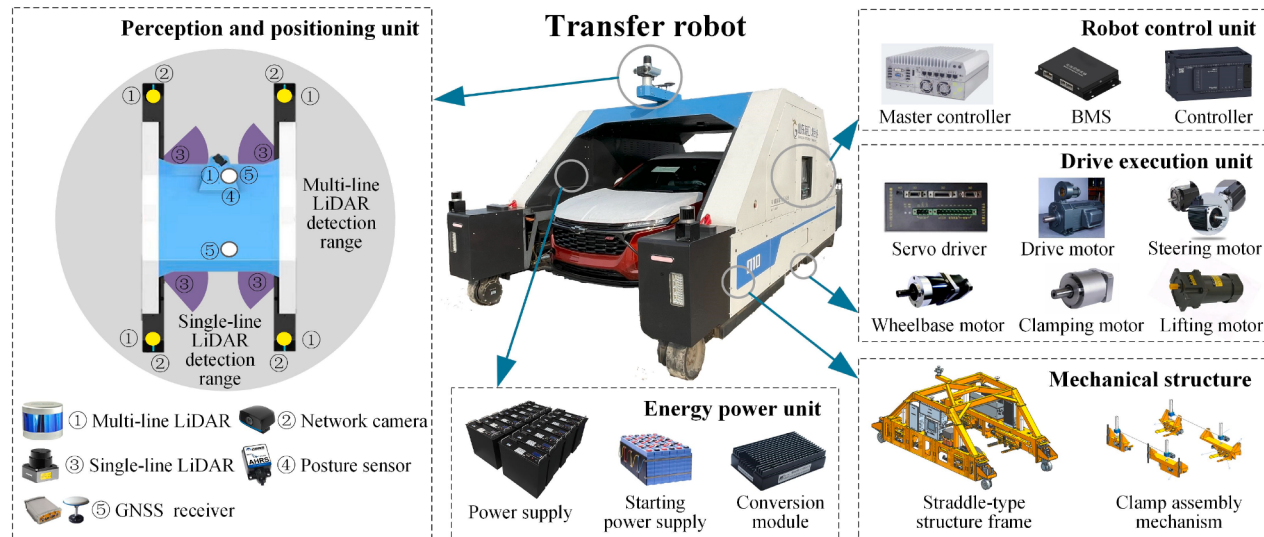


Fig. 4. Commercial vehicle automatic transfer robot composition.

Table 1
Basic Motion Parameters of Transfer Robot.

Descriptive	Value
Weight	6 t
Length × Width × Height	6 m × 3 m × 2.8 m
Maximum Speed	25 km/h
Maximum Load	2.5 t
Steering Angle	360°
Operating Wheelbase Range	2.6 m - 3.1 m

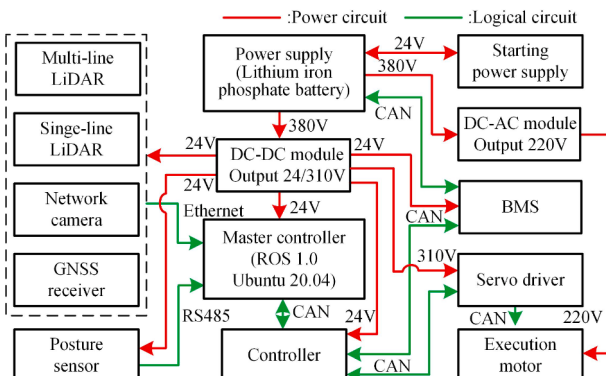


Fig. 5. Electrical architecture of commercial vehicle transfer robot.

servo driver converts control signals from the underlying controller into motor commands, which are sent to each motor. The drive motor and steering motor manage the robot's movement and steering, while the remaining motors handle vehicle clamping and lowering in accordance with control instructions.

The robot's electrical architecture, illustrated in Fig. 5, shows data transmission between the perception and positioning unit and the robot control unit using Ethernet and RS485 serial communication protocols. Communication between the drive execution unit and the robot control unit is facilitated through the CAN protocol. Both the power system and starting power supply utilize lithium iron phosphate batteries, managed by a battery management system (BMS). The BMS optimizes power based on the battery's state of charge, temperature, and power distribution.

2.4. System software architecture

As shown in Fig. 6, the system software mainly consists of two main components: the cloud scheduling and planning module and the robot perception and control module. The cloud scheduling and planning module comprises five layers: application, planning, access, command, and basic services. It operates on two servers, providing integration with the port production task management and control system. Through its modular, layered design, the system facilitates task scheduling, path planning, real-time monitoring, command control, intelligent charging, and anomaly alerts. The robot perception and control module, deployed on each autonomous transfer robot, consists of five layers as well: data, perception, planning, control, and basic services. Built on the Robot Operating System (ROS), this module handles local path planning, data communication, sensor data acquisition, target positioning, path tracking, and operation control.

Both modules share a common planning layer for integrated robot-cloud control. In cases where the robot module loses communication with the cloud system, the robot can continue operating autonomously, leveraging its task management, multi-robot coordination, and path planning capabilities.

In addition, the system software supports real-time monitoring of each robot's sensors, actuators, and key functional modules. A two-level emergency response mechanism—faults and warnings—is employed to trigger alerts upon detecting anomalies. Faults, such as critical sensor failures, communication disruptions, or server crashes, require immediate shutdown and reporting. Warnings, including partial LiDAR failures or low-frequency module heartbeats, do not interrupt operations due to system redundancy; they are logged and handled after task completion. As sensor and actuator usage varies across mission phases, the system dynamically adjusts alert criteria to ensure both safety and efficiency throughout the operation.

3. Cloud scheduling planning

The layout of the port yard and its roads is highly flexible, and the vehicle parking conditions are complex. This section proposes a cloud scheduling framework for a commercial vehicle transfer robot, featuring independent four-wheel drive and steering. The framework enables dynamic and efficient task assignment and multi-robot path planning, tailored to the unpredictable parking configurations of commercial vehicles in the yard. By leveraging this flexible yard environment, the framework enhances overall operational efficiency.

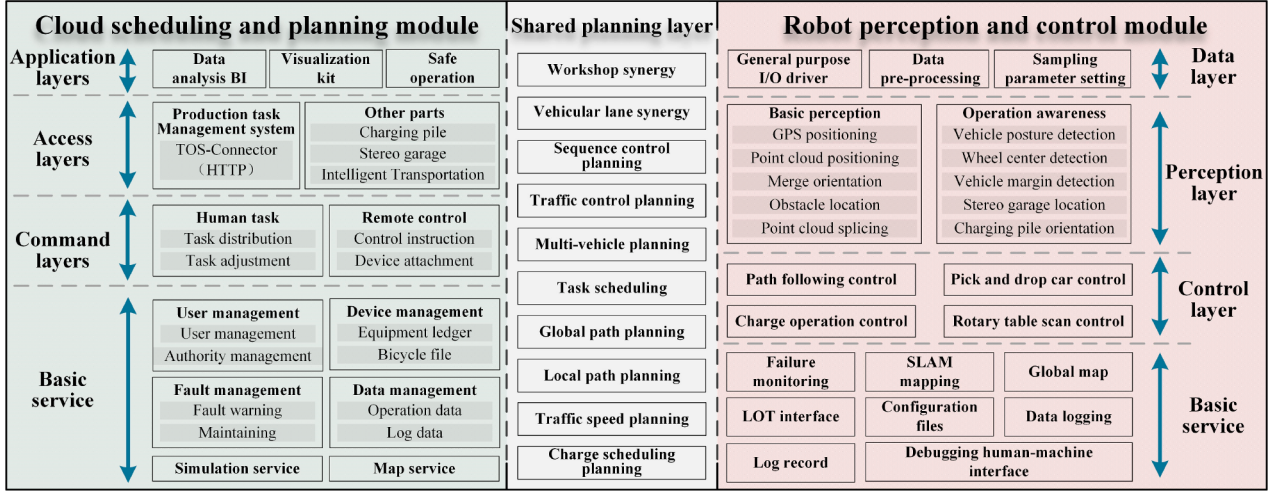


Fig. 6. Software architecture of robot system for autonomous transfer of commercial vehicles.

3.1. Task assignment method based on adaptive particle swarm genetic algorithm

To optimize the assignment of transfer robots to transfer tasks in the confined spaces of the port, an adaptive particle swarm genetic algorithm is proposed to address the robot task assignment problem. Traditional static or deterministic methods struggle with combinatorial complexity, task dynamics, and multiple conflicting objectives of such environments. By combining the global search ability of particle swarm optimization with the local refinement of genetic algorithms, it efficiently explores high-dimensional solution spaces while avoiding premature convergence.

The algorithm employs an integer encoding method to represent particles. Based on the total number of tasks, the number of robots, and the task dimensions, the robot assignment and task execution order are determined. To evaluate the quality of the task allocation, a multi-objective optimization function, defined in Eq. (1), is used as the fitness function for different particle positions. The A* search algorithm is applied to compute the distance cost for each robot as it travels from the starting position to each task position. Additionally, the angular difference between the robot's heading from the starting position to the first task position, and between subsequent task points in the execution sequence, is used to estimate the robot's mode-switching cost. Since the scheduling problem aims to minimize the objective function, the lower the fitness value, the better the task assignment scheme.

$$f_{cost} = \alpha_1 f_{mdis} + \alpha_2 f_{adis} + \alpha_3 f_{swi}, \quad (1)$$

where f_{mdis} is the cost of the farthest distance traveled by a single robot, f_{adis} represents the cost of the total distance traveled by all robots, f_{swi} denotes the total motion mode switching cost, and $\alpha_1, \alpha_2, \alpha_3$ are the weight of the three costs.

After initializing the particle swarm, the speed and position of the particles are updated using Eq. (2), with inertia parameters adaptively adjusted through iterative evolution and the degree of particle convergence.

$$\begin{cases} v_{i,t+1}^d = \omega_a v_{i,t}^d + c_1 r_1 (p_{i,best}^d - x_{i,t}^d) + c_2 r_2 (g_{best}^d - x_{i,t}^d) \\ x_{i,t+1}^d = x_{i,t}^d + v_{i,t}^d, \end{cases} \quad (2)$$

$$\omega_a = \omega_{max} - \frac{(\omega_{max} - \omega_{min}) \cdot t}{T} + \gamma \frac{F_{g,t}}{F_{a,t}}, \quad (3)$$

$$F_{a,t} = \frac{1}{N} \sum_{i=1}^N F_{i,t}, \quad (4)$$

where $x_{i,t}^d = (x_{i,t}^1, x_{i,t}^2, \dots, x_{i,t}^d)$ represent the position of the i th iteration, $v_{i,t}^d = (v_{i,t}^1, v_{i,t}^2, \dots, v_{i,t}^d)$ represent the velocity of the i th iteration, $p_{i,best}^d = (p_{i,best}^1, p_{i,best}^2, \dots, p_{i,best}^d)$ respectively represent the local optimal position of the i th particle respectively represent the local optimal position of the i th particle and $g_{best}^d = (g_{best}^1, g_{best}^2, \dots, g_{best}^d)$ represent the global optimal position in the particle swarm up to the t th iteration, r_1 and r_2 are uniform random numbers in [0,1], c_1 and c_2 are learning factors, ω_{max} and ω_{min} are respectively the maximum and minimum value of inertia weight, T is the maximum number of iterations, N is the number of particles, $F_{g,t}$ is the fitness of the global optimal position in the particle swarm of the t th iteration, $F_{a,t}$ is the average fitness value of the particle swarm at the t th iteration, γ is the particle aggregation coefficient, and $F_{i,t}$ represents the fitness value of the i th particle at the t th iteration.

To prevent the algorithm from converging to a local optimum, N pairs of particles are randomly selected from the current swarm as parents for crossover. Two fragments are randomly chosen from each particle and swapped to generate new particles. These newly generated particles undergo random mutation with a certain probability. Upon completing the crossover and mutation, both the new particles and the original swarm are sorted based on fitness. Following the principle of elite retention, the best particles are preserved, and the iterative process moves to the next generation of the swarm (Fig. 7).

The whole process is shown in Fig. 8. The particle swarm is initialized according to the above rules, and the fitness value of each particle at its initial position is calculated. The velocity and position of each particle are then updated. Subsequently, crossover and mutation are applied, and the process is iterated step by step. When the number of iterations

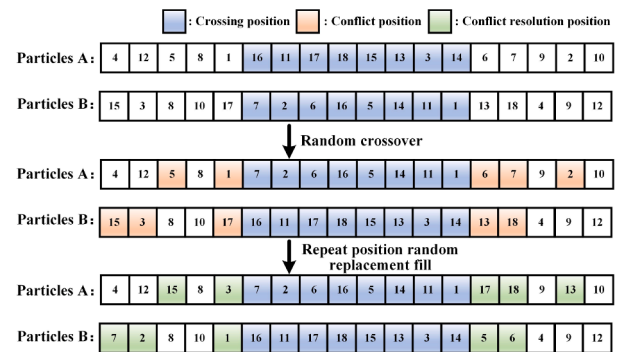


Fig. 7. Schematic diagram of the particle cross mutation process.

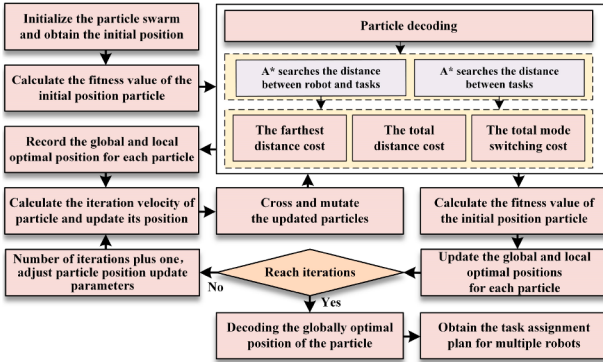


Fig. 8. The flow of adaptive particle swarm genetic algorithm.

reaches the predefined limit, the optimal particle solution is decoded and the transfer tasks of multiple robots are obtained.

3.2. Enhanced conflict search path planning algorithm under kinematic constraints

To achieve conflict-free path planning for multiple transfer robots in an open yard environment, a conflict search path planning algorithm is proposed, as illustrated in Fig. 9. This algorithm is based on the port environment map, the kinematic model of the transfer robots, and the positions of both the commercial vehicles and the transfer robots. It redefines the traditional concepts of “parking space” and “road” in the yard. Following preset rules, lanes are dynamically planned in real-time within available areas of the yard. Once the low-level planner identifies feasible paths for each transfer robot, the high-level system traverses these paths, detects conflicts, and translates them into constraints for further low-level planning. The process iterates until all paths are conflict-free, enabling the transfer robots to find the optimal conflict-free routes for moving the vehicles in the flexible yard environment.

To ensure the absolute safety of the commodity vehicles, the following rules are enforced for movement within the yard: transfer robots are only permitted to cross when at least three rows or three columns in the

yard are free of vehicles. Additionally, when a “lane” is designated as part of a transfer robot’s path, it becomes exclusively occupied by that robot, preventing other robots from using or planning along the same lane. During crossing, if the robot is moving longitudinally, it maintains its normal driving state; however, if moving laterally, it is restricted to exiting the yard horizontally and is prohibited from switching movement modes within the yard.

The low-level planning layer integrates the real-time updates of internal and external lanes within the yard and employs a hybrid A* algorithm that accounts for kinematic constraints. Compared with conventional methods, the algorithm incorporates the robot’s kinematic models under lateral and rotational motion modes. By explicitly accounting for motion constraints, it improves the robot’s maneuverability and motion feasibility. As shown in Eq. (5), the cost function g applies different penalties for retreating, lateral movement, self-rotation, and Ackerman steering. Additionally, the orientation cost from the current node to the endpoint is incorporated into the cost function h in Eq. (6). To further improve pathfinding speed in confined spaces, the algorithm introduces an adaptive heuristic weight factor ξ in Eq. (7), which adjusts dynamically based on the distance between the robot’s current position and the target point, balancing the tradeoff between optimality and solving speed.

$$g(s) = g(s_f) + \lambda_{turn} dist(s_f, s) + \lambda_{swi} dist(s_f, s), \quad (5)$$

$$h(s, s_{goal}) = h_0(s, s_{goal}) + h_h(s, s_{goal}), \quad (6)$$

$$f(s) = g(s) + \xi * h(s, s_{goal}), \quad (7)$$

where $g(s)$ is the path cost of the robot from the starting position to the current position, $h(s, s_{goal})$ is the estimated cost of the robot from the current position to the end position, $f(s)$ is the estimated cost of the robot from the starting position to the end position, $g(s_f)$ represents the cumulative cost of the parent node, $dist(s_f, s)$ represents the distance cost from the current node to the parent node, λ_{turn} represents the turning penalty factor, λ_{swi} represents the motion mode switch penalty factor, $h_0(s, s_{goal})$ is the Manhattan distance from the current position to the end position, $h_h(s, s_{goal})$ represents the orientation cost from the current node to the parent node, and ξ is the adaptive heuristic weight factor, when $\xi = 1$, the solution is complete, when $\xi > 1$, it is suboptimal, but it can be solved faster.

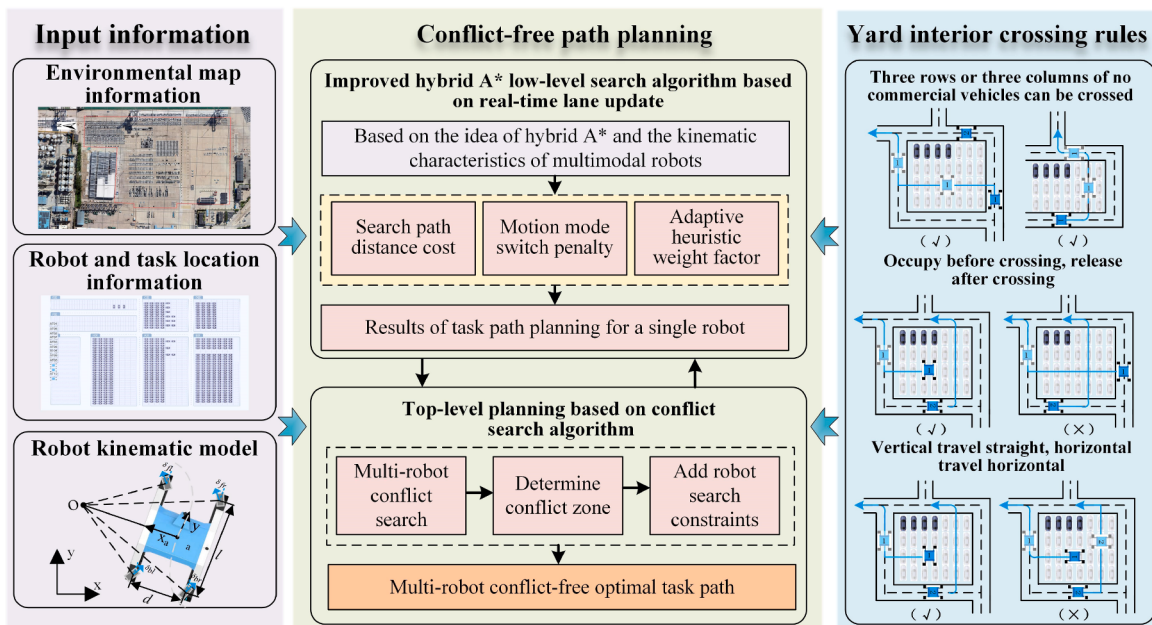


Fig. 9. Multi-robot path conflict-free planning schematic.

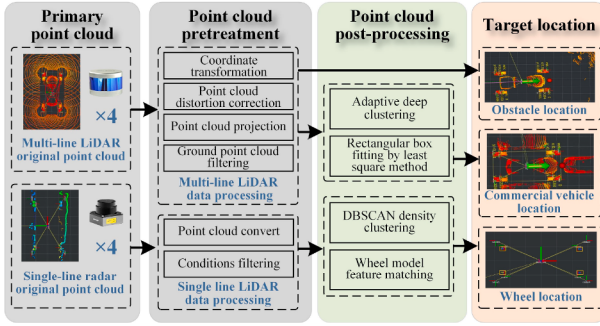


Fig. 10. Multi-stage sensor fusion target location algorithm framework.

4. Robotic pick-and-place operation

The commercial vehicles are densely parked in the yard, with fixed distances maintained on all sides—front, back, left, and right. These operations must also account for narrow spatial constraints and harsh, variable weather conditions. To address these challenges, this paper proposes a multi-stage sensor fusion algorithm for vehicle body positioning with multi-line LiDAR and wheel alignment with single-line LiDAR. It employs a virtual robot docking control algorithm to ensure precise vehicle placement and real-time adjustments. This approach effectively enhances the accuracy of vehicle positioning and docking in complex environments.

4.1. Commercial vehicle location based on multi-stage sensor fusion

To ensure the utmost safety during the autonomous transportation of commercial vehicles, as illustrated in Fig. 10, a multi-stage fusion algorithm for vehicle body positioning, orientation, and wheel alignment is implemented. This system utilizes surrounding multi-line LiDARs and internal single-line LiDARs. An event-trigger mechanism adjusts detection strategies based on the vehicle's status and its location. Specifically, in the pick-and-place vehicle approach phase, the commercial vehicle body is detected by surrounding multi-line LiDARs, while in the intersection phase, the single-line LiDAR is used to precisely locate and track the wheels. Additionally, the multi-line LiDARs assist with obstacle detection during navigation.

During the approach phase of the pick-and-place vehicle, commercial vehicle positioning relies on surrounding multi-line LiDARs. The position of the point cloud in the vehicle body coordinate system is calculated according to the position and attitude angle of the LiDARs in the vehicle body coordinate system. The motion distortion of the LiDARs is corrected according to the high frame rate information provided by the IMU. Subsequently, orderly projection of the point cloud onto a plane occurs, followed by filtering of ground points using angle and height thresholds based on neighboring points and seed growth methods. The point cloud distortion correction and projection formula are:

$$\begin{cases} \mathbf{R}_{t+\Delta t} = F(\omega(t + \Delta t) - \omega(t)) \\ \mathbf{P}_t = \mathbf{R}_{t+\Delta t} \mathbf{Q}_{t+\Delta t} + \mathbf{q}_{t+\Delta t}, \end{cases} \quad (8)$$

$$\begin{cases} \theta = \arcsin \frac{z_t}{\sqrt{x_t^2 + y_t^2 + z_t^2}}, h = \theta / \Delta \theta \\ \phi = \arcsin \frac{y_t}{\sqrt{x_t^2 + y_t^2}}, w = \phi / \Delta \phi, \end{cases} \quad (9)$$

where $\mathbf{R}_{t+\Delta t}$ represents the rotation matrix between the robot coordinate system at time t and the robot coordinate system at time $t + \Delta t$, $F(\cdot)$ represents the conversion function from Euler angles to rotation matrix, $\mathbf{P}_t = (x_t, y_t, z_t)$ is the position of the point at time t after distortion correction, $\mathbf{Q}_{t+\Delta t}$ represents the position of one of the points in the point cloud at time $t + \Delta t$, $\omega(t)$ represents the angular velocity of the robot at time t , $\mathbf{q}_{t+\Delta t}$ represents the translation vector of the robot at time $t + \Delta t$, θ and ϕ are the azimuth and zenith angles, $\Delta \theta$ and $\Delta \phi$ are the vertical and

horizontal resolutions of the LiDARs, respectively, (h, w) represents the position of the pixel point projected from the point cloud to the plane map.

Simultaneously, an adaptive deep clustering method is employed to group the angles between adjacent points in the processed point cloud. To account for angle calculations between diagonal points and the uneven vertical resolution of some point clouds, a more general angle calculation formula based on the cosine law is introduced to enhance the clustering method's applicability. Given that the commercial vehicle's shape is well-suited for rectangular frame fitting, key points are first extracted using convex hull calculation, and the point cloud is downsampled. The problem is then formulated as fitting a two-dimensional rectangular bounding box. The least squares method is applied to assess the fitting performance. Once the optimal rectangular frame is identified, the commercial vehicle's position and orientation are determined from the center coordinates and the direction of the fitted rectangle. The clustering decision condition and the objective function of rectangular frame fitting optimization are:

$$\beta = \arccos \frac{d^2 + d_1^2 - d_2^2}{2dd_1} > \lambda, \quad (10)$$

$$\begin{aligned} \text{minimize}_{\theta, c_1, c_2} & \sum_{i \in S} (x_i \cos \theta + y_i \sin \theta - c_s)^2 \\ & + \sum_{i \in Q} (-x_i \sin \theta + y_i \cos \theta - c_q)^2, \end{aligned} \quad (11)$$

$$\begin{aligned} \text{subject to } & S \cup Q = P \& S \cap Q = \emptyset \\ & c_s, c_q \in \mathbb{R} \quad 0^\circ \leq \theta < 90^\circ \end{aligned}$$

where β is the angle between two adjacent points in the point cloud, d is the distance between two adjacent points in the point cloud, d_1 is the distance between the farther point of the two points in the point cloud and the origin of the vehicle body, d_2 is the distance between the closer point of the two points in the point cloud and the origin of the vehicle body, and λ is the clustering threshold, which is automatically adjusted according to the distance between the target and the origin of the vehicle coordinate system. $P = \{p_i(x_i, y_i) \in \mathbb{R}^2 | i = 1, 2, \dots, m\}$ is a set of two-dimensional points on the same plane, S and Q are two disjoint sets, and θ is the rectangular orientation after fitting.

In the intersection phase, the single-line LiDARs locate wheels by first transforming coordinates and applying radius filtering to the original point cloud. Density clustering via the DBSCAN algorithm forms clusters, defining point cloud segments with wheel cross-section features. These segments match a predefined wheel model, yielding precise wheel position and orientation.

4.2. Predictive control for robot docking based on virtual transfer robot tracking

Once the target vehicle posture is obtained in real time, a robot docking prediction control algorithm based on virtual vehicle tracking is proposed. This algorithm uses the overall speed and steering angle of the transfer robot to control the robot in performing tasks such as pick-up and drop-off operations. The overall framework is illustrated in Fig. 11.

After identifying the commercial vehicle's location, a virtual transfer robot is positioned directly behind the actual vehicle, with its posture aligned to that of the commercial vehicle. The virtual robot is designed to approach the target vehicle from the rear. Simultaneously, the actual transfer robot is controlled to follow the virtual robot until it aligns with the vehicle to be picked up. During the vehicle drop-off stage, the virtual robot moves forward until a standard parking distance is maintained with the vehicle ahead. Considering the yard environment and task characteristics, a comprehensive speed planning model combined with a sliding average filter is employed to plan the speed. In this way, the commercial vehicle docking problem is transformed into the virtual transfer robot docking trajectory tracking problem, that is, the commercial vehicle docking can be realized by controlling the real transfer robot

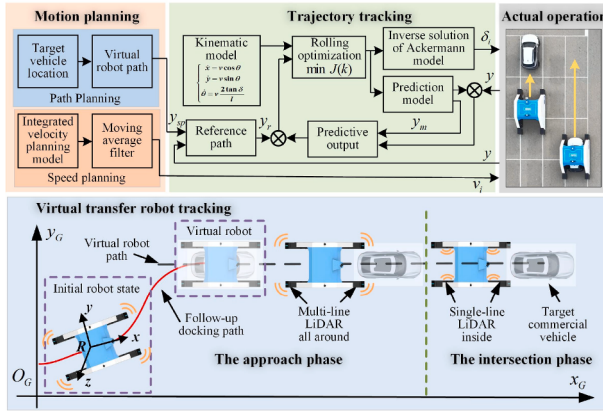


Fig. 11. Docking predictive control algorithm framework based on virtual transfer robot tracking.

to track the safe trajectory movement of the virtual robot. The motion trajectory of the virtual transport robot and the position of the virtual transport robot in the real robot coordinate system can be expressed as follows:

$$\begin{bmatrix} x_{vr} \\ y_{vr} \end{bmatrix} = \begin{bmatrix} x_{vr,0} \\ y_{vr,0} \end{bmatrix} + \begin{bmatrix} v_{vr} t \sin \theta_T \\ v_{vr} t \cos \theta_T \end{bmatrix}, \quad (12)$$

$$\begin{bmatrix} {}^R x_{vr} \\ {}^R y_{vr} \end{bmatrix} = \begin{bmatrix} {}^R x_T \\ {}^R y_T \end{bmatrix} + \begin{bmatrix} \cos \theta_R & \sin \theta_R \\ -\sin \theta_R & \cos \theta_R \end{bmatrix} \begin{bmatrix} x_T - x_{vr} \\ y_T - y_{vr} \end{bmatrix}, \quad (13)$$

where (x_{vr}, y_{vr}) is the position of the virtual robot, $(x_{vr,0}, y_{vr,0})$ represents the initial coordinates of the virtual robot in the world coordinate system, v_{vr} is the velocity of the virtual robot and θ_T represents the heading angle of the target commercial vehicle. $({}^R x_{vr}, {}^R y_{vr})$ is the relative position of the virtual robot in the real robot's coordinate system, $({}^R x_T, {}^R y_T)$ is the relative position of the target in the real robot's coordinate system, (x_T, y_T) is the position of the target and θ_R represents the heading angle of the real robot.

Given that the trajectory of the real transfer robot tracking the virtual robot involves a multi-variable, multi-constrained control problem, model predictive control is applied based on the kinematic model of the transfer robot to achieve accurate trajectory tracking. To ensure smooth operation and account for the actuator limitations of the transfer robot, constraints are placed on both the control input and its rate of change. The corresponding cost function is:

$$\begin{aligned} \text{minimize } & \sum_{i=1}^{N_p} \left\| \eta(k+i | k) - \eta_{ref}(k+i | k) \right\|_Q^2 \\ & + \rho \epsilon^2 + \sum_{j=0}^{N_c-1} \left\| \Delta \delta(k+j | k) \right\|_R^2, \end{aligned} \quad (14)$$

$$\text{subject to } \begin{aligned} & \delta_{\min} < \delta < \delta_{\max} \\ & \Delta \delta_{\min} < \Delta \delta < \Delta \delta_{\max} \end{aligned}$$

where Q and R are the weight matrices of control output and control input, ρ represents the weight factor, ϵ is the relaxation factor, N_p is the predicted value, N_c is the control range, $\eta(k+i | k)$ represents the i step predicted output of the prediction model, $\eta_{ref}(k+i | k)$ represents the i step reference trajectory of the prediction model, $\Delta \delta(k+j | k)$ is the i control increment, δ_{\min} and δ_{\max} are the minimum and maximum control values, respectively.

The solved control increment for the heading angle is then accumulated into the current control input, allowing the optimal heading angle for the next control cycle to be calculated as $\delta(k) = \delta(k-1) + \Delta \delta^*(k)$. Based on this, the steering motor speeds for each wheel are inversely calculated using the Ackerman steering model. Before generating the next control input, the current input is applied to the steering motor actuator, allowing the transfer robot to follow the trajectory and successfully dock with the commercial vehicle.

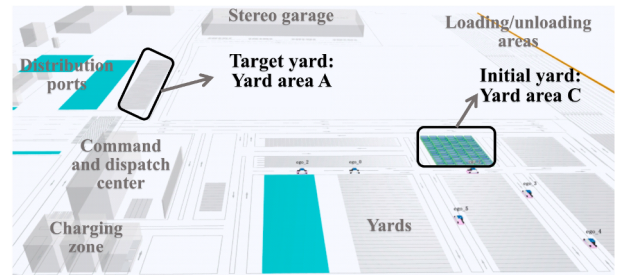


Fig. 12. Scenario design of multiple robots transporting commercial vehicles.

5. Deployment experiment

Field tests were conducted at the Ro-Ro Terminal in Yantai Port, Shandong, China, to validate the feasibility of the proposed robot system for autonomous commercial vehicle transfer, as well as the effectiveness of the cloud scheduling system and robotic operation systems. The tests involved multi-robot collaborative transfer of commercial vehicles test, robot pick-up and drop-off vehicles operations test, and complex harsh conditions operation test. Among them, the robot pick-up and drop-off vehicles operations test further includes the pick-up docking test, drop-off docking test, and the cyclic pick-up and drop-off accuracy test.

5.1. Multi-robot collaborative transfer of commercial vehicles test

5.1.1. Multi-robot transfer scenario setting

For evaluating the cloud scheduling planning method, as shown in Fig. 12, six transfer robots were deployed to move commercial vehicles from Yard area C to Yard area A, located near the distribution port. The distance between the C-area and M-area yards spans 200 m east-west and 150 m north-south. The port production task management system assigned the transfer tasks, while the cloud scheduling system handled task allocation and global path planning. Path instructions were then transmitted to each robotic operation system, enabling the transfer robots to autonomously complete the vehicle transfer tasks.

5.1.2. Result analysis of multi-robot transfer of commodity vehicles

A test was conducted to evaluate the multi-robot collaborative transfer of commercial vehicles within the designed transfer scenario. And during the test process, the feasibility of its algorithm and the overall transfer efficiency were evaluated by recording the task completion time and the trajectory traveled by the robot during the task execution. The transfer process is depicted in Fig. 13. Fig. 14 illustrates the path taken by the robots from their parking points to the yard. At the same time, Fig. 15 presents a portion of the trajectories for the robots performing pick-up and drop-off operations within the yard.

As shown in Fig. 14, six transfer robots depart from the parking point towards the yard. Due to the tight arrangement of commercial vehicles in the yard and the robots' straddle-seat pick-up method, conflicts may arise if adjacent robots attempt to pick up vehicles simultaneously. To prevent this, the scheduling plan ensures that Robot 1 to Robot 5 pick up vehicles with one commercial vehicle spacing between them. When Robot 6 arrives at the yard, Robot 1 to Robot 5 will have completed their pick-up tasks, and Robot 6 is scheduled to pick up the remaining vehicle between Robot 1 and Robot 2. According to the planned path, robots can navigate intersections either using Ackerman steering or by self-rotation. Given the limited space for posture adjustments due to densely parked vehicles, robots adjust their posture via self-rotation outside the yard before entering.

From the partial trajectory shown in Fig. 15(a) and (b), Robot 5 completes its pick-up task and heads towards the vehicle storage area, arriving at the storage point around the 400-second mark. After storing the vehicle, it returns to the yard for the next pick-up. Meanwhile, Robot 1

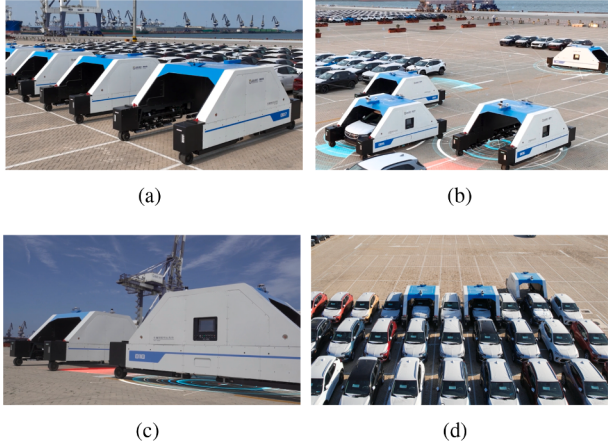


Fig. 13. Multi-robot transfer process: (a) Transfer robot initiating from parking point; (b) Coordinated movement of multiple robots on roads and yards; (c) Two robots yielding at the yard intersection; (d) Three transfer robots pick-up vehicles in the yard.

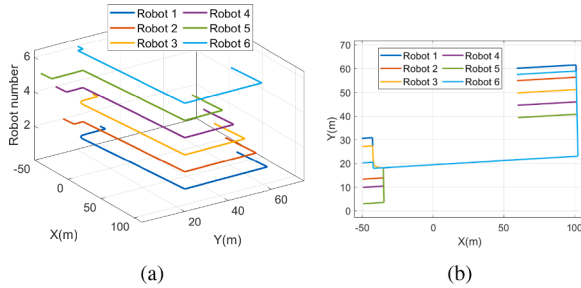


Fig. 14. The path of multiple robots from the parking spot to the yard to pick up the car: (a) Stereoscopic perspective; (b) Top-down perspective.

and Robot 2 arrive at the yard and begin their pick-up tasks before proceeding to the storage point. Simultaneously, Robot 3 and Robot 4 are on their way from the storage area to the pick-up area. After arriving, they pick up vehicles and proceed to the storage point. As illustrated in Fig. 15(c), although the X coordinates of multiple robots may be equal at certain moments, their Y coordinates remain distinct, ensuring that no two robots occupy the same position simultaneously. There is no deadlock at the intersection, and all robots maintain independent operation. Therefore, there is no conflict or deadlock during the entire commercial vehicle transfer process, which verifies the effectiveness of the proposed cloud scheduling planning algorithm.

During the commercial vehicle transfer test, the maximum speed of the transfer robot was set to 10 km/h, with an average time of 45 s for each vehicle pick-up and release. Six transfer robots successfully moved 30 commercial vehicles from the M area to the C area of the yard, completing the task in a total of 1 h, 50 min, and 56 s. In comparison, manual operation allows each worker to transfer only 3 vehicles per hour, involving multiple roles such as inspectors, tally clerks, traffic controllers, vehicle drivers, and commercial vehicle drivers. The single robot achieves 91 % of the transfer efficiency of the single human operator in the same amount of time. Furthermore, the robots can operate continuously for 2 to 3 times longer than human workers, significantly reducing exhaust emissions, improving environmental conditions, and streamlining the complexities of manual processes.

5.2. Robot pick-up and drop-off vehicles operations test

5.2.1. Robot pick-up vehicles docking test

To verify the effectiveness of the robot pick-up vehicles method, the single-vehicle picking function test of the transfer robot is designed. Record the lateral deviation and angular deviation between the robot

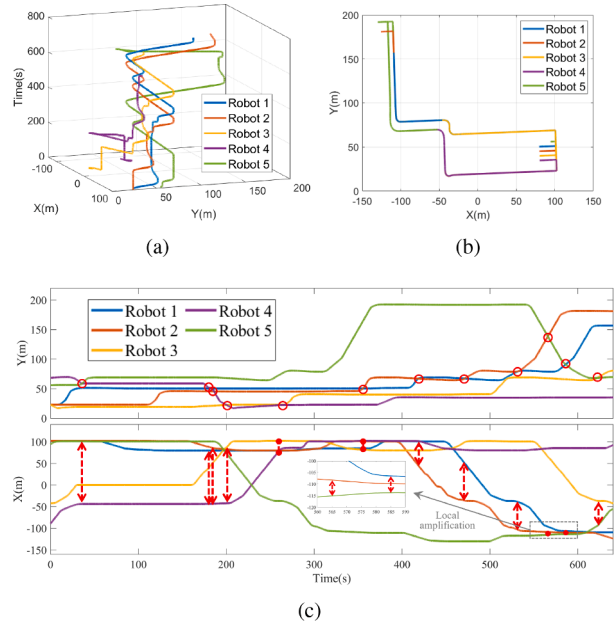


Fig. 15. Trajectory of multiple robots during partial pick-up and drop-off operations in a yard: (a) Stereoscopic perspective; (b) Top-down perspective; (c) Trajectory x-coordinate and y-coordinate curves of multiple robots.

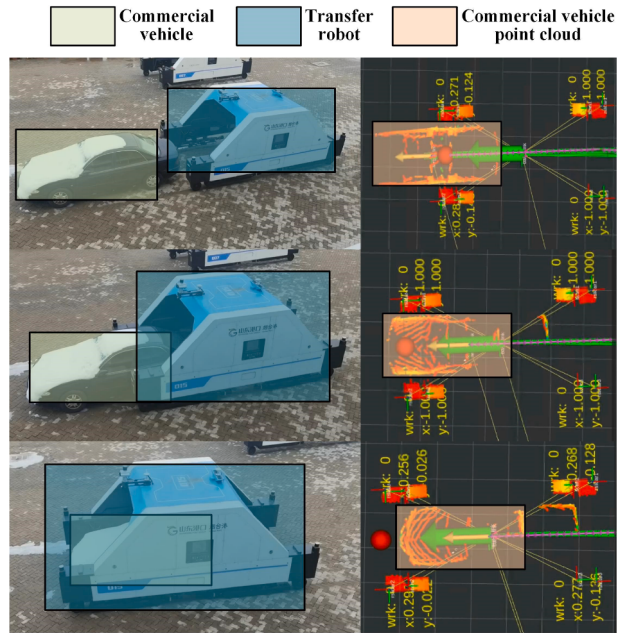


Fig. 16. Transfer robot pick-up docking process.

and the vehicle during the docking process, and further calculate the docking error of the vehicle through the lateral and longitudinal distances between four single-line LiDARs and the wheels. The docking and clamping process is illustrated in Figs. 16 and 17.

As illustrated in Fig. 16, during the approach phase of vehicle pick-up for docking, the transfer robot detects and localizes the commercial vehicle using multi-line LiDARs. In the intersection phase, single-line LiDARs are used to locate the wheels for precise docking, allowing the robot to decelerate and stop accurately. Once stationary, the clamp's height is adjusted, and the rear single-line LiDARs detect the wheel position to refine the wheelbase alignment further. The clamping mechanism is controlled through a sequence of operations, including downing, clamping, and lifting the clamp, completing the process in 45 s. To further examine the dynamics of the vehicle pick-up docking, Fig. 18(a)



Fig. 17. The process of the transfer robot holding the commercial vehicle.

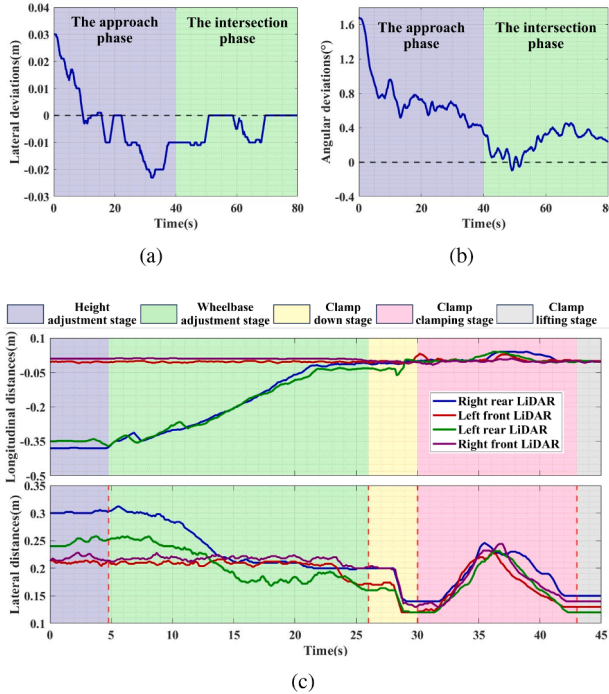


Fig. 18. The docking and clamping process of the transfer robot taking the vehicle: (a) Lateral deviations of the robot during docking; (b) Angular deviations of the robot during docking; (c) Lateral and longitudinal distances of the inner four single-line LiDARs to the wheels.

and (b) presents the lateral and angular deviations of the robot during the pick-up vehicle process. Additionally, Fig. 18(c) shows the lateral and longitudinal distances between the inner four single-line LiDARs and the wheels of the commercial vehicle during clamping.

As shown in Fig. 18, during the approach phase of vehicle pick-up, the transfer robot conducts path planning and tracking based on the commercial vehicle pose detected and located by multi-line LiDAR, achieving significant position adjustment. This reduced the lateral deviation between the transfer robot and the vehicle from 0.03 m to 0.01 m and the angular deviation from 1.7° to 0.4°. After switching to single-line LiDARs for wheel localization, more precise adjustments were made, eventually eliminating lateral deviation and reducing angular deviation to 0.3°. After completing the vehicle pick-up and docking, the robot lifts the commercial vehicle through five stages: height adjustment, wheelbase adjustment, clamp down, clamp clamping, and clamp lifting. During parking, the commercial vehicle's front wheel is located by the front single-line LiDARs. In the wheelbase alignment stage, the rear single-line LiDARs adjusts the distance to the rear wheels, aligning the clamping mechanism with the rear wheels. When the clamp descends, the left LiDARs adjusts the distance to the wheel from 0.18 m to 0.12 m, and the right LiDARs adjusts from 0.2 m to 0.14 m, accounting for tire shape. During clamping, influenced by the wheel hub's shape, the lateral distance briefly increases before decreasing again. After clamping and

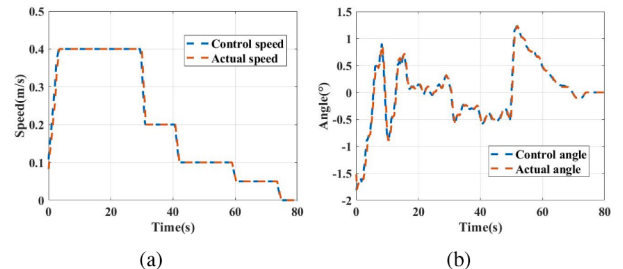


Fig. 19. The speed and control angle tracking curve output by the transfer robot: (a) Speed curve; (b) Control angle curve.

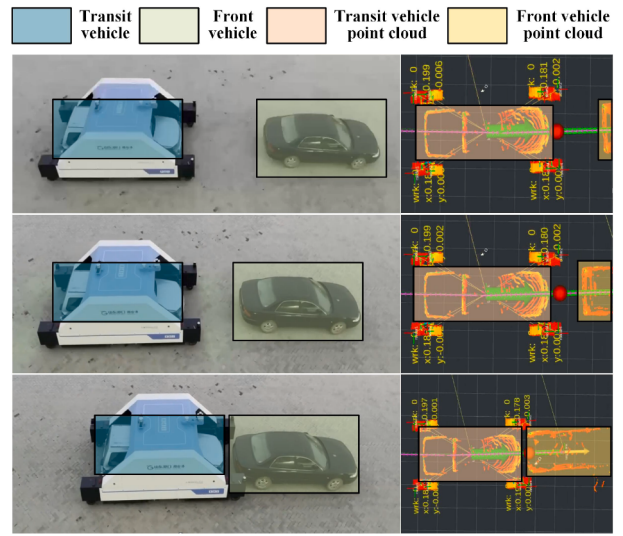


Fig. 20. Transfer robot drop-off docking process.

lifting, the final lateral distances between the left front, right front, left rear, and right rear single-line LiDARs and the corresponding wheels are 0.13 m, 0.14 m, 0.12 m, and 0.15 m, respectively, with longitudinal distances of 0 m. Both lateral and longitudinal positioning deviations are less than 0.02 m, achieving centimeter-level accuracy in positioning and vehicle pick-up.

The speed and control angle tracking curve output by the transfer robot during the vehicle pick-up and docking process is shown in Fig. 19. The speed curve demonstrates that the robot adjusted its speed based on environmental conditions at various stages. The speed and angle response times are controlled within 0.2 s, ensuring accurate tracking of control commands and meeting the required response time and precision for control accuracy.

5.2.2. Robot drop-off vehicles docking test

To verify the effectiveness of the robot drop-off vehicles method, the single-vehicle placement function test of the transfer robot is designed. The recorded indicators are consistent with those of the robot pick-up vehicles test. The vehicle picking test process is shown in Figs. 20 and 21.

During vehicle placement, the transfer robot utilizes multi-line LiDARs to locate the position of the commercial vehicle ahead. Through trajectory planning and tracking control, the robot accurately docks the commercial vehicle behind the vehicle in front. The vehicle is then placed by lowering the clamp, releasing the clamp, rising the clamp, adjusting the wheelbase, and finally adjusting the clamp height through logic control. The entire vehicle lowering and releasing process takes 45 s. To further analyze the characteristics of the vehicle placement and docking, Fig. 22(a) and (b) presents the lateral and angular deviations of the transfer robot during the drop-off vehicles process, while Fig. 22(c)



Fig. 21. The process of the transfer robot unloading the commercial vehicle.

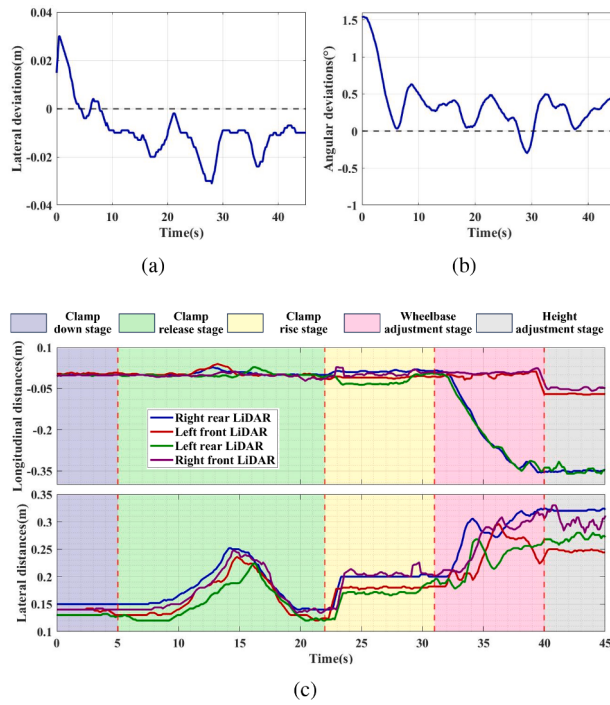


Fig. 22. The docking and release process of the handling robot placing the vehicle: (a) Lateral deviations of the robot during docking; (b) Angular deviations of the robot during docking; (c) Lateral and longitudinal distances of the inner four single-line LiDARs to the wheels.

provides the lateral and longitudinal distances between the four inner single-line LiDARs and the wheels during releasing.

As shown in Fig. 22, during the docking stage, the transfer robot adjusts its position based on data from the preceding commercial vehicle, detected by the multi-line LiDARs. Through continuous trajectory planning and tracking control, the lateral deviation is reduced from 0.03 m to 0.01 m, and the angular deviation is corrected from 1.5° to 0.5° . Additionally, the process of adjusting the clamp during vehicle placement is the reverse of the vehicle pick-up procedure. The commercial vehicle is lowered through logical control, and the clamp is reset. Unlike vehicle pick-up, the clamp does not require high precision during vehicle placement, allowing for a straightforward reset.

5.2.3. Cyclic pick-up and drop-off accuracy test

To further verify the accuracy of the vehicle pick-up and placement process, a reliability test scenario was constructed. Multiple commercial vehicles were arranged to simulate the actual operating conditions of the yard, and the transfer robot was tasked with performing a series of pick-up and drop-off vehicle cycle tests. The cycle test process is illustrated in Fig. 23. Two transfer robots completed 30 cycles of pick-up and drop-off vehicle tests. The lateral, longitudinal, and angular deviations of each test process are recorded as shown in Fig. 24, and the accuracy is summarized in Table 2.

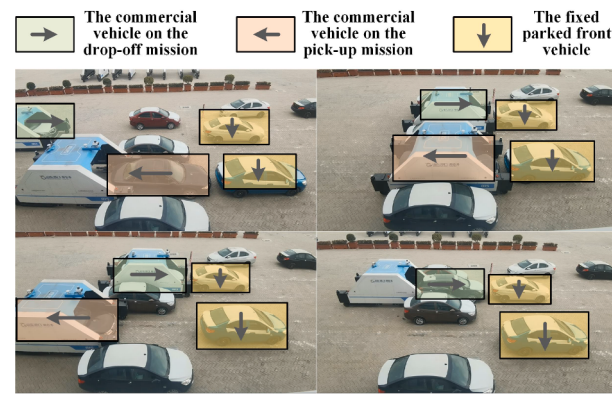


Fig. 23. The process of cyclic pick-up and drop-off vehicles testing by the transfer robot.

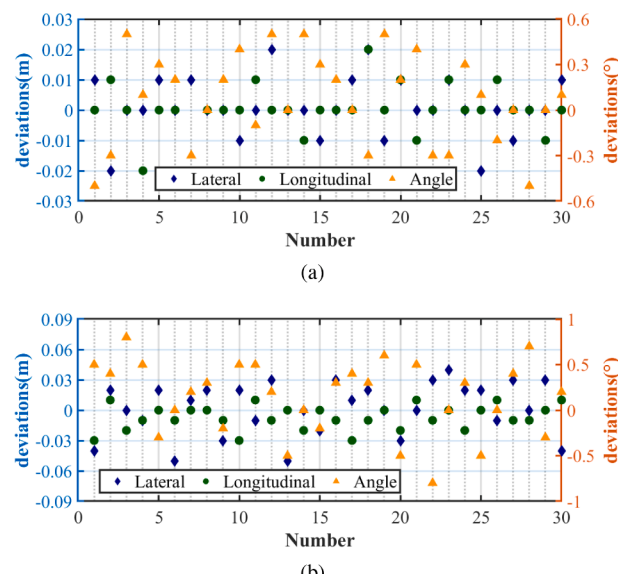


Fig. 24. Deviation results of 30 pick-up and drop-off vehicles tests: (a) Pick-up vehicles process; (b) Drop-off vehicles process.

Table 2
Deviation results of pick-up and drop-off vehicles.

Stage	Lateral deviation		Longitudinal deviation		Angle deviation	
	Max	Mean	Max	Mean	Max	Mean
Pick-up	0.02	0.01	0.02	0.01	0.50	0.25
Drop-off	0.03	0.01	0.05	0.02	0.80	0.36

In summary, after 30 cycles of testing, the maximum lateral, longitudinal, and angular deviations during the vehicle pick-up stage were 0.02 m, 0.02 m, and 0.5° , respectively, with average deviations of 0.01 m, 0.01 m, and 0.25° . During the vehicle placement stage, the maximum lateral, longitudinal, and angular deviations during the vehicle placement stage were 0.03 m, 0.05 m, and 0.8° , respectively, with average deviations of 0.01 m, 0.02 m, and 0.36° , achieving centimeter-level positioning accuracy for pick-up and placement operations. The larger deviations during the vehicle placement stage were attributed to the use of both multi-line and single-line LiDARs for joint positioning in the pick-up stage, while only multi-line LiDARs were used for positioning during the placement stage.

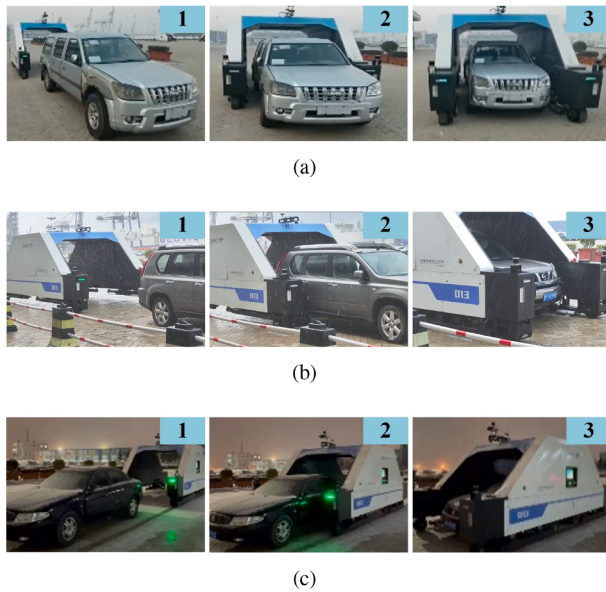


Fig. 25. Operation results in complex harsh conditions: (a) Foggy weather conditions; (b) Rainy weather conditions; (c) Snowy weather conditions.

5.3. Complex harsh conditions operation test

To verify the reliability of the transfer robot's operation in complex harsh conditions, the vehicle retrieval function of the transfer robot was tested under three harsh conditions: foggy weather conditions, rainy weather conditions, and snowy weather conditions. The results are shown in Fig. 25.

As illustrated in Fig. 25, the transfer robot demonstrates robust performance in adverse weather conditions such as fog, rain, and snow. The system effectively filters out irrelevant environmental point cloud noise, maintaining high vehicle pick-up accuracy and reliably completing docking operations. It should be noted that testing was not conducted under extremely severe conditions, as manual operations are typically suspended in such environments.

6. Discussion

Intelligent unmanned systems are widely used in warehousing logistics, container transshipment, and ore transportation due to their autonomy, intelligence, and unmanned features. However, research on autonomous transfer of commercial vehicles remains primarily focused on small-scale indoor operations, with many outdoor solutions facing limitations. In this context, this paper innovatively proposes an autonomous transshipment solution tailored for Ro-Ro terminals. This solution integrates the characteristics of large weight, high cargo value, and compact parking of commercial vehicles to create a robot system that includes intelligent transfer robots, a cloud scheduling system, and robotic operation systems. We examine the cloud scheduling planning algorithm and the robotic pick-and-place operation algorithm. To our knowledge, this intelligent logistics solution for Ro-Ro terminals is the first of its kind globally, effectively addressing a significant research gap in this field.

In our research, compared with traditional warehousing logistics, commercial vehicles, which are larger and heavier with no outer packaging protection, necessitate a focus on safety amid complex outdoor terrains. Compared to container transshipment, the commercial vehicle scenario is more intricate, with variable yard and road distributions and dynamic locations for pick-up and placement. Additionally, unlike other scenarios where goods are directly “placed” onto transfer equipment, autonomous transfer of commercial vehicles requires precise docking and clamping by the transfer robot, with no margin for error to avoid

losses. This paper targets the unique challenges of commercial vehicle transfer at Ro-Ro terminals, proposing a robot system for autonomous transfer and conducting on-site deployment tests to validate the effectiveness of the system and its key technologies. Due to limited space, this paper offers a holistic solution to inspire and inform technicians in related fields, without delving deeply into each technology, focusing instead on the overall framework and key technologies.

As of this study, although the proposed autonomous transfer robot system is currently deployed only at Ro-Ro terminals, it encompasses several cutting-edge interdisciplinary domains, including robotics, intelligent transportation, scheduling and planning, perception and localization, and systems control. The key technologies involved are modular and transferable, offering potential for broader application in other domains. The overall solution can be extended to outdoor environments such as commercial vehicle logistics hubs and automotive manufacturing plants. Moreover, it provides a viable framework for the autonomous transfer of large and heavy cargo in open areas, thereby promoting the integration of emerging technologies with traditional industries and accelerating the intelligent transformation of logistics operations.

7. Conclusion

This paper presents the first autonomous commercial vehicle transfer solution, integrating a straddling dual-body, large-load electric robot, cloud scheduling system, and robotic operation systems—replacing manual operations at Ro-Ro terminals. Among them, a task allocation method based on an adaptive particle swarm genetic algorithm and a motion-constrained, conflict-aware path planning algorithm are proposed to ensure conflict-free cooperative transfer of multiple robots in both task assignment and path planning. Furthermore, we develop a multi-stage fusion algorithm for vehicle body positioning, orientation, and wheel alignment, along with a predictive control algorithm for robot docking based on virtual transfer vehicle tracking, ensuring precise docking with commercial vehicles during all stages of pick-up and drop-off. The system was deployed at the Ro-Ro terminal of Yantai Port in Shandong, China, and underwent systematic testing, including multi-robot collaborative transfer, autonomous vehicle pick-up/drop-off, and operation under harsh conditions. A 30-cycle pick-and-place test showed that the robot achieved a docking accuracy within 0.02 m and an angular deviation of 0.5 degrees. In the tested scenario, its handling efficiency reached 91 % of manual operations, and in real production, its continuous working time was 2–3 times that of human workers. These results confirm the system's effectiveness and practicality, address a key research gap, and support the intelligent transformation of commercial vehicle logistics.

Although the robots have achieved 91 % of manual handling efficiency and can operate 2–3 times longer than human workers, there remains room for further optimization. Future improvements may include enabling multiple robots to pick up vehicles simultaneously from both the front and rear of the yard, allowing forward exit using the straddle structure, and accelerating the clamping process. In addition, the integration of large pre-trained and generative AI models is expected to enhance multi-robot perception and autonomous decision-making.

Data availability

Data will be made available on request.

CRediT authorship contribution statement

Lin Zhang: Writing original – draft, Visualization, Validation, Methodology, Formal analysis; **Yongkang Xu:** Writing-review & editing, Methodology; **Jinge Si:** Writing-review & editing, Visualization; **Runjiao Bao:** Validation, Formal analysis; **Yichen An:** Software, Data Curation; **Shoukun Wang:** Project administration, Funding acquisition; **Junzheng Wang:** Supervision, Conceptualization..

Declaration of competing interest

The authors declare that they have no known competing financial interests or personal relationships that could have appeared to influence the work reported in this paper.

Acknowledgements

This work is supported by the National Natural Science Foundation of China (No. 62473044), the BIT Research and Innovation Promoting Project (No. 2024YCXZ007), and the Fundamental Research Funds for the Central Universities (No.2024CX06023).

References

- Bonab, S. R., Ghoushchi, S. J., Deveci, M., & Haseli, G. (2023). Logistic autonomous vehicles assessment using decision support model under spherical fuzzy set integrated Choquet Integral approach. *Expert Systems with Applications*, 214, 119205.
- Cai, W., Zhang, M., Yang, Q., Wang, C., & Shi, J. (2023). Long-range UWB positioning-based automatic docking trajectory design for unmanned surface vehicle. *IEEE Transactions on Instrumentation and Measurement*, 72, 1–12.
- Cao, Y., Yang, A., Liu, Y., Zeng, Q., & Chen, Q. (2023). AGV dispatching and bidirectional conflict-free routing problem in automated container terminal. *Computers & Industrial Engineering*, 184, 109611.
- Carlos, B. B., Williams, M., & Pelourdeau, B. (2023). Real-time NMPC for an automated valet parking with load-based safety constraints and a path-parametric model. In *2023 IEEE/RSJ International conference on intelligent robots and systems (IROS)* (pp. 10006–10013). IEEE.
- Chen, X., He, S., Zhang, Y., Tong, L. C., Shang, P., & Zhou, X. (2020). Yard crane and AGV scheduling in automated container terminal: A multi-robot task allocation framework. *Transportation Research Part C: Emerging Technologies*, 114, 241–271.
- Chen, X., Li, F., Jia, B., Wu, J., Gao, Z., & Liu, R. (2021). Optimizing storage location assignment in an automotive ro-ro terminal. *Transportation Research Part B: Methodological*, 143, 249–281.
- Chen, Y., & Li, Z. (2022). An effective approach of vehicle detection using deep learning. *Computational Intelligence and Neuroscience*, 2022(1), 2019257.
- Ding, N., Ming, R., & Wang, B. (2023). Efficient convex-hull-based vehicle pose estimation method for 3D LiDAR. *Transportation Research Record*, (03611981241250027).
- Endo, M., Hirose, K., Hirata, Y., Kosuge, K., Kanbayashi, T., Oomoto, M., Akune, K., Arai, H., Shinoduka, H., & Suzuki, K. (2008). A car transportation system by multiple mobile robots-iCART. In *2008 IEEE/RSJ International conference on intelligent robots and systems* (pp. 2795–2801). IEEE.
- Gong, L., Wu, Y., Gao, B., Sun, Y., Le, X., & Liu, C. (2022). Real-time dynamic planning and tracking control of auto-docking for efficient wireless charging. *IEEE Transactions on Intelligent Vehicles*, 8(3), 2123–2134.
- Jiao, G., Huang, M., Song, Y., Li, H., & Wang, X. (2024). Container loading problem based on robotic loader system: An optimization approach. *Expert Systems with Applications*, 236, 121222.
- Jin, X., Yang, H., He, X., Liu, G., Yan, Z., & Wang, Q. (2023). Robust LiDAR-based vehicle detection for on-road autonomous driving. *Remote Sensing*, 15(12), 3160.
- Kashiwazaki, K., Yonezawa, N., Endo, M., Kosuge, K., Sugahara, Y., Hirata, Y., Kanbayashi, T., Suzuki, K., Murakami, K., & Nakamura, K. (2011). A car transportation system using multiple mobile robots: iCART II. In *2011 IEEE/RSJ International conference on intelligent robots and systems* (pp. 4593–4600). IEEE.
- Kottinger, J., Almagor, S., & Lahijanian, M. (2022). Conflict-based search for multi-robot motion planning with kinodynamic constraints. In *2022 IEEE/RSJ International conference on intelligent robots and systems (IROS)* (pp. 13494–13499). IEEE.
- Li, J., Tinka, A., Kiesel, S., Durham, J. W., Kumar, T. K. S., & Koenig, S. (2021). Life-long multi-agent path finding in large-scale warehouses. In *Proceedings of the AAAI conference on artificial intelligence* (pp. 11272–11281). (vol. 35).
- Li, K. X., Li, M., Zhu, Y., Yuen, K. F., Tong, H., & Zhou, H. (2023). Smart port: A bibliometric review and future research directions. *Transportation Research Part E: Logistics and Transportation Review*, 174, 103098.
- Li, W., Cai, L., He, L., & Guo, W. (2024). Scheduling techniques for addressing uncertainties in container ports: A systematic literature review. *Applied Soft Computing*, 111820.
- Lina, W., Zhihao, L., Ying, Q., Yue-feng, G., & Wancong, W. (2020). Research on automatic driving transfer mode of commercial vehicles by special channel based on 5G. *Logistics Research*, (2), 52–63.
- Liu, W., Kuang, Z., Zhang, Y., Zhou, B., He, P., & Li, S. (2025). An effective hybrid genetic algorithm for the multi-robot task allocation problem with limited span. *Expert Systems with Applications*, 280, 127299.
- Liu, Y., Wang, H., Liu, B., Chen, L., Wang, Y., & Chen, H. (2022). Learning-based compound docking control for UAV aerial recovery: Methodology and implementation. *IEEE/ASME Transactions on Mechatronics*, 28(3), 1706–1717.
- Naeem, D., Gheith, M., & Eltawil, A. (2023). A comprehensive review and directions for future research on the integrated scheduling of quay cranes and automated guided vehicles and yard cranes in automated container terminals. *Computers & Industrial Engineering*, 179, 109149.
- Pan, T., Yan, J., Zhou, S., Cai, Y., & Lu, C. (2020). Spin-type forward motion mode based on double steering wheel parking AGV. *Industrial Robot: the international journal of robotics research and application*, 47(5), 777–787.
- Polack, P., Dallen, L.-M., & Cord, A. (2020). Strategy for automated dense parking: How to navigate in narrow lanes. In *2020 IEEE International conference on robotics and automation (ICRA)* (pp. 9196–9202). IEEE.
- Ran, L., Liu, B., Zhang, G., & Cheng, Y. (2025). An improved particle swarm optimization algorithm for berth allocation and time-variant quay crane scheduling problem during an emergency. *Expert Systems with Applications*, 269, 126406.
- Slanina, Z., Pergl, I., & Kedron, P. (2022). Automated guided vehicle control system for automated parking purposes. *IFAC-PapersOnLine*, 55(4), 362–367.
- Tsolakis, N., Zissis, D., Papaefthimiou, S., & Korfiatis, N. (2022). Towards AI driven environmental sustainability: An application of automated logistics in container port terminals. *International Journal of Production Research*, 60(14), 4508–4528.
- Wang, J., Wang, L., & Han, H. (2024). A knowledge-driven cooperative coevolutionary algorithm for integrated distributed production and transportation scheduling problem. *IEEE Transactions on Automation Science and Engineering*, 22, 7435–7448.
- Wang, Y., Shan, M., Yue, Y., & Wang, D. (2020). Autonomous target docking of nonholonomic mobile robots using relative pose measurements. *IEEE Transactions on Industrial Electronics*, 68(8), 7233–7243.
- Wang, Z., Lyu, X., Zhang, J., Wang, P., Zhong, Y., & Shi, L. (2025). MAC-planner: A novel task allocation and path planning framework for multi-robot online coverage processes. *IEEE Robotics and Automation Letters*, 10(05), 4404–4411.
- Weifeng, L., Qicheng, L., & Yanjie, S. (2023). Design analysis and test of folding box for vehicle transport. *China Water Transport*, 23(08), 75–79.
- Wen, L., Liu, Y., & Li, H. (2022). CL-MAPF: Multi-agent path finding for car-like robots with kinematic and spatiotemporal constraints. *Robotics and Autonomous Systems*, 150, 103997.
- Wu, Y., Wang, L., & Chen, J.-f. (2024). A branch-and-bound enhanced cooperative evolutionary algorithm for the hybrid seru system scheduling considering worker heterogeneity. *IEEE Transactions on Evolutionary Computation*.
- Xu, F., Wang, Z., Wang, H., Lin, L., & Liang, H. (2023). Dynamic vehicle pose estimation and tracking based on motion feedback for LiDARs. *Applied Intelligence*, 53(2), 2362–2390.
- Xu, Y., Chen, Z., Deng, C., Wang, S., & Wang, J. (2024). LCDL: Towards dynamic localization for autonomous landing of unmanned aerial vehicle based on LiDAR-camera fusion. *IEEE Sensors Journal*, 24(16), 26407–26415.
- Yang, L., Ge, Y., Zheng, Y., & Zeng, H. (2025). Cross-area scheduling and conflict-free path planning for multiple robots in non-flat environments. *Expert Systems with Applications*, 272(5), 126767.
- Zang, Z., Song, J., Lu, Y., Zhang, X., Tan, Y., Ju, Z., Dong, H., Li, Y., & Gong, J. (2023). A unified framework integrating trajectory planning and motion optimization based on spatio-temporal safety corridor for multiple AGVs. *IEEE Transactions on Intelligent Vehicles*, 9(1), 1217–1228.
- Zang, Z., Zhang, X., Song, J., Lu, Y., Li, Z., Dong, H., Li, Y., Ju, Z., & Gong, J. (2024). A coordinated behavior planning and trajectory planning framework for multi-ugvs in unstructured narrow interaction scenarios. *IEEE Transactions on Intelligent Vehicles*.
- Zhang, D., Chen, F., & Mei, Z. (2023a). Optimization on joint scheduling of yard allocation and transfer manpower assignment for automobile RO-RO terminal. *Transportation Research Part E: Logistics and Transportation Review*, 177, 103256.
- Zhang, X., Ming, X., & Chen, Z. (2018). Integration of AI technologies and logistics robots in unmanned port: A framework and application. In *Proceedings of the 4th international conference on robotics and artificial intelligence* (pp. 82–86).
- Zhang, Z., Chen, J., & Guo, Q. (2023b). Application of automated guided vehicles in smart automated warehouse systems: A survey. *CMES-Computer Modeling in Engineering & Sciences*, 134(3), 1529–1563.
- Zhao, F., Song, L., Jiang, T., Wang, L., & Dong, C. (2024). A policy-based meta-heuristic algorithm for energy-aware distributed no-wait flow-shop scheduling in heterogeneous factory systems. *IEEE Transactions on Systems, Man, and Cybernetics: Systems*.
- Zhou, S., Yang, H., Lashkov, I., Chen, C., Xu, H., Zhang, G., & Yang, Y. (2025). Deep learning-based vehicle detection and tracking from roadside LiDAR data through robust affinity fusion. *Expert Systems with Applications*, 279, 127338.